The effect of high-flux H plasma exposure with simultaneous transient heat loads on tungsten surface damage and power handling

G.G. van Eden[1], T.W. Morgan[1], H.J. van der Meiden[1], J. Matejicek[2], T. Chraska[2], M. Wirtz[3] and G. De Temmerman[4]

[1] FOM Institute DIFFER, Dutch Institute for Fundamental Energy Research, Association EURATOM-FOM, 3430 BE Nieuwegein, The Netherlands
[2] Institute of Plasma Physics, Association EURATOM-IPP, 182 00 Prague 8, Czech Republic
[3] Forschungszentrum Jülich GmbH, Institute of Energy and Climate Research Microstructure and Properties of Materials (IEK-2), EURATOM Association, 52425 Jülich, Germany
[4] ITER Organization, Route de Vinon sur Verdon, CS 90 096, 13067 Saint Paul-lez-Durance, France

E-mail: g.g.vaneden@differ.nl

Abstract. The performance of the full-W ITER divertor may be significantly affected by the interplay between steady-state plasma exposure and transient events. To address this issue, the effect of a high-flux H plasma on the thermal shock response of W to ELM-like transients has been investigated. Transient heating of W targets is performed by means of a high-power Nd:YAG laser with simultaneous exposure to H plasma in the linear device Magnum-PSI. The effects of simultaneous exposure to laser and plasma has been compared to those sequentially and to laser only. Transient melting is found to be aggravated during plasma exposure and to occur at lower heat flux parameters. Roughness and grain growth are observed to be driven by peak temperature, rather than by the loading conditions. The temperature evolution of the W surface under a series of transients is recorded by fast infrared thermography. By accounting for changes in the reflectivity at the damaged surface as measured by ellipsometry, a reduction in power handling capabilities of the laser/plasma affected W is concluded. The evidence of reduced power handling of the W surface under conditions as described here is of great concern with respect to the durability of W PFCs for application in fusion devices.

PACS numbers: 28.52.Fa, 52.40.Hf, 52.55.Rk, 52.55.Fa

1. Introduction

It has now been decided that ITER will be equipped with a full-tungsten (W) divertor from the start of operation. One of the crucial factors for the application of W as a Plasma-Facing-Component (PFC) is ensuring durability under the expected extreme conditions of heat and particle flux.

In particular, the type-I ELMs expected for ITER are of great concern for the PFCs because of their highly repetitive nature (1-25 Hz) and high energy loss from the core plasma (up to 10 % of the total plasma energy) that is subsequently deposited on the divertor plates on a sub-ms timescale [1]. Before replacement of the divertor armour material, the targets are expected to endure $>10^6$ ELMs with a peak energy density up to 10 MJ m^{-2} [2]. These transients are expected to induce strong thermal stresses and may lead to unacceptable levels of erosion of the ITER divertor [3]. Material degradation such as plastic deformation due to the impact of transients are predicted to affect the PFC microstructure [4] leading to a degradation of its thermal response and mechanical strength over time. In turn, the resulting modifications of surface topology and properties may have a serious impact on plasma operation [5].

Previous work has mostly focused on replicating ELMs using transient heating methods alone [6, 7, 8, 9]. Thermal shock tests using either electron guns or a pulsed laser are found to yield similar results [10] and proved to serve as a method to study ELM-induced material degradation. From this, it is observed that recrystallization, grain growth, roughening, cracking and melting evolves as function of number of pulses, transient power load and base temperature of the PFC.

Specific loading conditions for surface cracking have been identified (e.g. 1000 pulses of 1 ms at $F_{HF} = 12$ MJ m^{-2} s$^{-1/2}$ at a base temperature of 700 °C [11]) which could lead to a significant reduction in PFC lifetime, while even for low heat flux parameters ($F_{HF} = 6$ MJ m^{-2} s$^{-1/2}$) significant damage such as roughening and crack formation can accumulate over a large number of pulses (10^6) through fatigue [6].

The addition of plasma irradiation has been found to have a significant effect compared to thermal loading alone. Pre-implantation of high-flux hydrogen (H) plasma is observed to lead to an increased damage level after laser irradiation compared to only laser loading [8]. On the other hand, when high power plasma pulses were used to simulate ELMs at Pilot-PSI, the power delivered to the target was found to be mitigated by the shielding effect of outgassed neutrals [12].

Despite these efforts, the additional effect of an ITER-relevant plasma on the thermal shock response of W and its power handling capability is still not well understood. Since additional damage mechanisms may be triggered by synergistic effects between the plasma and transients that could lead to a reduced performance of the PFCs, the effects of a high-flux plasma on the thermal shock response of W needs to be assessed.

In this report, investigations of the damage effects of transients produced by a pulsed Nd:YAG laser on W, both in absence and presence of a steady-state high-flux H

plasma in the linear device Magnum-PSI are described. A ms laser was used to replicate type-I ELMs more realistically than the nanosecond laser used in previous studies. The evolution of roughness, grain growth and changes in power handling capabilities of the W surface with progressing number of pulses and the additional effect of plasma on this were assessed.

2. Experimental methods

2.1. Setup

Experiments were performed in the linear plasma generator Magnum-PSI, designed to study plasma-wall-interactions in ITER-like divertor regimes [13]. A schematic overview of the target- and source chamber of this machine including laser injection system is shown in figure 1. The plasma source was operated using a DC current of 150-190 A and H gas flow in the range 5.0-7.0 Pa m^3 s^{-1}. By switching on the axial magnetic field (up to 1.9 T [14]) the plasma was confined into a beam hitting the target (biased to -38 V) resulting in a particle flux of 1.5-3x10^{23} m^{-2} s^{-1}, electron temperature 1-2 eV and a heat flux density in this case up to ∼2.5 MW m^{-2} in the centre of the plasma column.

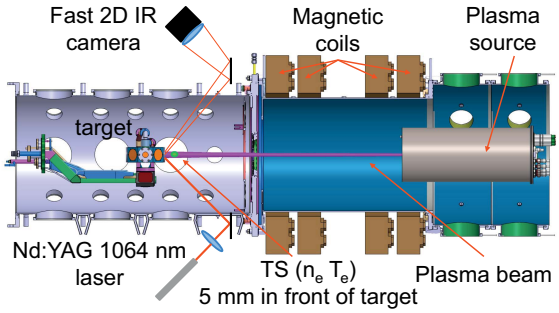

Figure 1: Schematic view of Magnum-PSI in combination with the Nd:YAG laser.

Transient heating was performed using a 1064 nm high power fibre-coupled Nd:YAG laser (LASAG FLS 352-302) with a pulse duration of 1 ± 0.1 ms, 10-25 Hz repetition rate and 1-21 kW input power. The spatial profile of the laser beam exiting the fiber can be approximated by a gaussian (FWHM ≈ 1 mm) and its temporal profile is a nearly-square waveform. This shape is maintained upon arrival at the target, based on analysis using the IR camera. The laser beam propagates through a lens, mirror and window over a distance of ∼0.5 m in atmospheric air just before entering the vacuum target chamber. The total energy transmission (α_T) of the laser coupling into the target chamber of Magnum-PSI was found to be 75 ± 1%, based on measurements using a calorimeter just before the target position.

2.2. Samples

The exposed samples were polycrystalline rolled tungsten discs (Plansee AG, Austria) of 30 mm diameter and 1 mm thickness. The discs exhibit 99.97 % purity and were

polished to a mirror finish having roughness of 0.05 µm with a typical grain size of 2-3 µm in diameter. The targets were ultrasonically cleaned in ethanol and acetone and subsequently out-gassed and stress-relieved by heating up to 1000 °C for 60 minutes in vacuum. The samples were clamped onto a water-cooled copper holder using tantalum clamping rings. The backside of the targets were actively cooled by water at 20 °C during exposure.

2.3. Diagnostics and post-mortem analysis

The electron temperature and density of the plasma were obtained by Thomson Scattering (TS) [15] at a position 5 mm in front of the target. The evolution of the sample surface temperature was traced for each consecutive laser pulse in detail by using a fast infrared camera (FLIR SC7500MB) operated using a frame rate up to 6.3 kHz. A temperature dependent emissivity calibration for W [16] was used to convert the raw signal to temperature.

Post-mortem analysis of the surface morphology of exposed targets was performed using Scanning Electron Microscopy (SEM) equipped both with a secondary electron (SE) and backscattered electron (BSE) detector at the Institute of Plasma Physics AS CR in Czech Republic. Furthermore, reflectivity measurements using ellipsometry were carried out at ASML labs in Eindhoven to quantify changes in absorbance as a function of the loading conditions.

Surface roughness was quantified by laser profilometry (Polaris from UBM Messtechnik GmbH) at Forschungszentrum Jülich (FZJ) measuring maximum surface elevations of 500±0.01 µm using the reflectivity of a 670 nm laser. Around the circular loaded area, a square surface of $2.2\times2.2\,\mathrm{mm}^2$ was scanned with a lateral resolution of 10 µm in both the x- and y-direction, yielding the arithmetic roughness parameter R_a. This parameter is defined as the arithmetic average of the deviation from the average height along the examined surface [17]. Finally, the grain size in the centre of the damaged laser spots was assessed by measuring and averaging the diameter of multiple grains at the surface in high resolution SEM images obtained using backscattered electrons (BSE detection).

2.4. Determining laser heat flux parameter

The laser spot size (A) was defined as the circular area enclosed by the FWHM of the Gaussian heat pulse that was obtained from IR processing. By integrating a 2D Gaussian, the circular area within the diameter of the FWHM contains 50 % of the entire volume. Therefore, the energy within the FWHM contains 50 % of all input energy (E_{in}). The average heat flux parameter (F_{HF}) [4], expressed in $\mathrm{MJ\,m^{-2}\,s^{-1/2}}$, arriving within the FWHM of the laser deposited area was then calculated by taking into account transmission losses in both fiber and injection system (α_T), absorption at

target (α_W), spot size (A) in m^2 and set pulse duration (t) in s:

$$F_{HF} = \frac{1}{2}\alpha_T \alpha_W \frac{E_{in}}{A\sqrt{t}}. \quad (1)$$

The actual energy transferred from the laser to the target is greatly affected by changes in target absorption. This issue is addressed in the next section. The heat flux parameter is used in this study as damage thresholds (roughening, cracking, melting, boiling) occur at similar values for different test facilities [18] which enables direct comparisons among them to be made.

The temperature increase induced by the transient (ΔT) is directly proportional to F_{HF} and the thermophysical properties of the material and is approximated by the following 1D model

$$\Delta T = F_{HF} \frac{2}{\sqrt{\pi k C_v \rho}}, \quad (2)$$

where k denotes thermal conductivity, C_v specific heat and ρ the density. A decrease in any of these parameters leads to a reduced loading requirement to reach a damage threshold [4, 18]. The model assumes exposure to a uniform heat flux on the surface whereas the incident laser profile in our experiments is Gaussian. The error associated with this is however small as we are interested in the maximum surface temperature which could be spatially resolved down to ∼150 µm by the IR camera. Compared to the size of the FWHM which is ∼1 mm, a uniform heat flux over the width of a single pixel can be assumed and the 1D model is thus appropriate.

The actual heat flux parameter of the laser pulse deposited at the target for given laser input energy was calculated using equation (1). Subsequently, the temperature rise was approximated by equation (2) while assuming the following thermal properties for W at room temperature (RT): k = 177 W m^{-1} K^{-1}, C_v = 134 J kg^{-1} K^{-1}, ρ = 19.300 kg m^{-3}. k decreases by 55 % whereas C_v increases by 33 % from from RT to 2000 °C. Hence, as the square root is taken of the product of these parameters, equation (2) is expected to provide a reasonable approximation, even at high temperatures.

Figure 2 shows the calculated laser-induced temperature rise in comparison to the measured temperature increase from the IR camera averaged over the first 10 pulses for given F_{HF}. The error associated to F_{HF} is due to uncertainties in spot size, optics transmission and absorbance. The error in the pulse duration is negligible in comparison to the previously mentioned contributions. As only the peak temperatures of the first few thermal cycles are taken into account, the surface is assumed to be barely plastically deformed and thus pristine reflectivity (58 %) is assumed. As can be seen, a good agreement between the measured and predicted temperature based on the heat flux parameter as defined in equation (1) is found which indicates that the IR calibration is accurate.

2.5. Surface reflectivity

As surface height deformations are induced on a similar scale as the operation wavelength of the laser (∼1 µm), the surface reflectivity is expected to change. With this, the

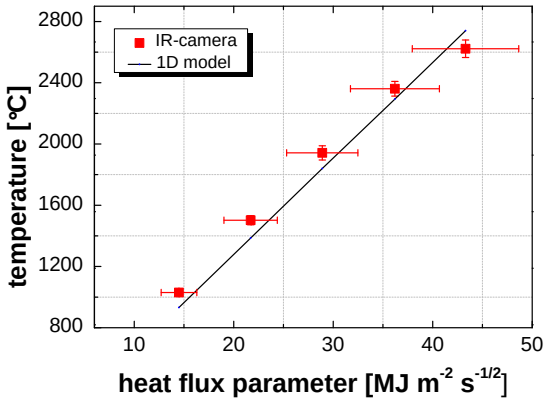

Figure 2: Average peak temperature of the first set of 10 pulses reached during the powerscan of the laser. The calculated peak temperatures as predicted by the 1D model are shown by the line.

actual heat flux parameter deposited on the target is changed as well. In order to disambiguate the changes in reflectivity from those in the thermal properties of the sample, the changes in reflectivity could be indirectly inferred from post-mortem ellipsometry analysis yielding the dielectric properties (n and k) locally at the laser-affected spots. From this, the total reflectivity R_{tot} (defined as the sum of specular- and diffusive reflectivity) was calculated using the Fresnel equations. Results for pristine W and affected positions due to the laser power scan are shown in figure 3.

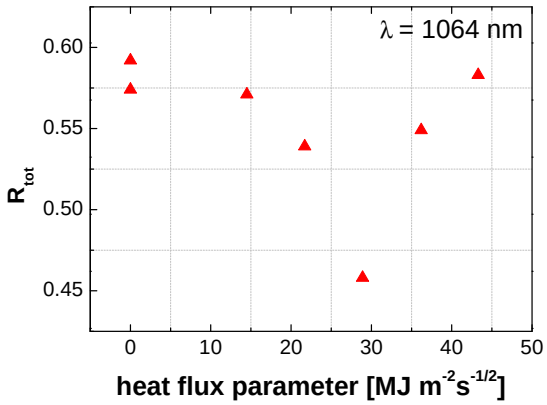

Figure 3: Total reflectivity (R_{tot}) for 1064 nm radiation at laser affected spots after being exposed to 100 laser pulses for heat flux parameters as indicated, obtained by ellipsometry analysis.

A total reflectivity of 58 % is determined for pristine W samples at 1064 nm. With increasing F_{HF}, the total reflectivity decreases from 58 % to 46 % at $F_{HF} = 29$ MJ m^{-2} s$^{-1/2}$. For F_{HF} >29 MJ m^{-2} s$^{-1/2}$, where the surface melted, the reflectivity approaches again the undamaged value. Melting of the surface smoothes severely roughened grains as observed from SEM images (see next section), thus increasing the total surface reflectivity [19]. The changes in reflectivity as a result of simultaneous

plasma and laser irradiation appeared to be minimal: a maximum relative deviation from the pristine reflectivity of 3 % on the area exposed to plasma and 100 pulses at $F_{HF} = 25.2\ MJ\,m^{-2}\,s^{-1/2}$ was found. Changes in reflectivity for the other combined 100 pulse exposures were found to be negligible.

2.6. Exposure conditions

First, the effect of laser irradiation alone was investigated using a wide range of pulse numbers and heat flux parameters. After that, targets were exposed to pulsed laser and plasma simultaneously. In order to disentangle the effect of the elevated surface temperature from the effect caused by plasma-surface interactions during plasma exposure, laser pulses were also applied to an externally heated sample in the absence of plasma. Using this method, surface temperatures similar to those reached during steady-state plasma operation were achieved. Details of the loading conditions can be found in table 1.

experiment	**F_{HF}** [$MJ\,m^{-2}\,s^{-1/2}$]	**pulses** [#]	**rep. rate** [Hz]	**T_{base}** [°C]	**H fluence** [$\times 10^{24}\,m^{-2}$]	**series**
laser only	37.5	1 - 5000	10	20	0	A
	14.5 - 43.3	100	10	20	0	B
	15.2 - 26.5	100	10	440	0	C
	13.4 - 16	1000	25	600	0	D
plasma+laser	13.9 - 32.2	100	10	240	12.4 - 13.7	E
	11.2 - 25.2	100	10	450	3.9 - 4.6	F
	10.6 - 15	1000	25	300	11.6 - 12.1	G
	5.4 - 15.1	1000	25	600	8.5 - 14.8	H

Table 1: Loading conditions of W samples exposed during this study. The pulse duration was held constant at 1 ms.

3. Results and discussion

3.1. Surface modifications

Surface modifications induced by laser irradiation of samples at RT (series A and B) were examined by post-mortem SEM images taken at the centre of the exposed areas. Surface damage as a result of a an increasing number of pulses at $F_{HF} = 37.5\ MJ\,m^{-2}\,s^{-1/2}$ are shown in figure 4. Exposure to such a heat flux parameter heats the surface up to ∼2500 °C at the centre of the laser spot during 1 ms, causing steep temperature gradients between the irradiated area and surrounding bulk. This thermal shock leads to mechanical stresses and plastic deformation after cool-down. Grain growth is observed in the centre of the laser spot after a single pulse (4b) when compared to the pristine surface (4a). Grain growth proceeds as the number of pulses increases and the surface

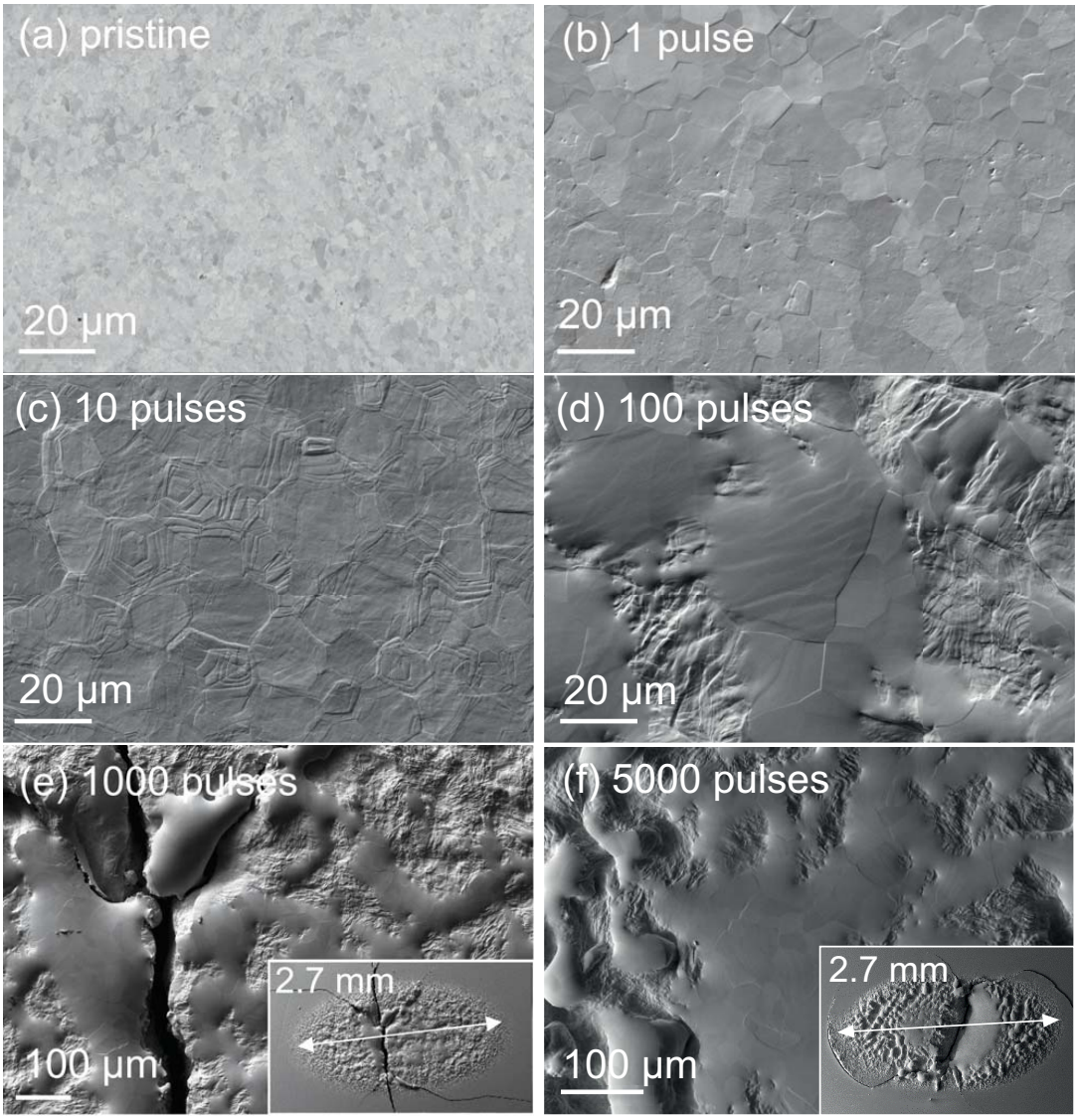

Figure 4: SEM images of W surface at the centre of the laser deposition area after applying pulses at 37.5 MJ m^{-2} s$^{-1/2}$ for a number of pulses as indicated (series A).

becomes gradually rougher after 10 pulses (4c). Discontinuous melted areas consisting of a few grains within the irradiation spot are visible for a number of pulses >100 and grow with increasing number of transients (4d). For >1000 pulses, an increase in the melted surface area is accompanied by the formation of large cracks (typically ∼20 µm wide and ∼200 µm deep) as found from line profile measurements. As surface melting and cracking at this heat flux parameter is only observed for ≥100 and ≥1000 pulses respectively, a progression of damage with the number of pulses is clear.

Surface temperatures both measured during this exposure and calculated from the 1D model indicate peak temperatures (T_{peak}) of ∼2500 °C (figure 2), which is significantly below the melting threshold (T_m) of W of ∼3420 °C [20]. It is proposed that severe roughening leads to protruded grains that suffer from a locally reduced

heat dissipation capability which are over-heated when the laser strikes, thus passing T_m while the surrounding surface temperature is below this [21, 22]. These individual melted grains are too small to be resolved by the IR camera as it measures distances of about 1/6 of the FWHM of the heat pulse which corresponds to ∼150 µm.

Although a minor effect, the emissivity is known to be affected by surface roughening. An increase in emissivity up to ∼4 % was revealed for a recrystallized and roughened surface compared to pristine W. By taking this into account, the real surface temperature should be even slightly lower than the measured temperature and is therefore not an explanation for the gap between the measured surface temperature and the melting threshold.

Over the course of a large number of pulses (≥1000), T_{peak} increases gradually with each consecutive pulse and IR measurements give $T_{peak} > T_m$ after a few hundred pulses. The large number of pulses is found to modify the surface such that its heat dissipation capability is reduced over a spatial range large enough to be resolved by the IR camera and thus >150 µm. This is confirmed by the size of the melted areas after 1000 and 5000 pulses in SEM images 4e and 4f which are >200 µm.

Next to varying the number of pulses per laser position, the effect of laser power is investigated by varying this at a fixed number of 100 pulses per loaded area (series B). Figure 5 shows the resulting surface damage. It is found that loading at $F_{HF} = 14.5\ \mathrm{MJ\,m^{-2}\,s^{-1/2}}$ does not lead to significant surface modifications (5a). Roughening of the surface is pronounced when loading $>20\ \mathrm{MJ\,m^{-2}\,s^{-1/2}}$. The onset of melting is observed for heat fluxes $>36\ \mathrm{MJ\,m^{-2}\,s^{-1/2}}$ (5c) and the formation of a contiguous melt pool consisting of large grains happens $>43\ \mathrm{MJ\,m^{-2}\,s^{-1/2}}$ (5d). The peak temperature measured at the centre of the positions where melting is observed is ∼2480 °C and ∼2690 °C respectively, again lower than the melting threshold which shows the surface temperature to be spatially non-uniform.

No cracking is observed on any of the areas subjected to 100 pulses (only after 1000 and 5000 pulses at $F_{HF} = 37.5\ \mathrm{MJ\,m^{-2}\,s^{-1/2}}$ while the sample was at RT). This result contrasts with previously performed experiments at FZJ using the same high power laser system by Wirtz *et. al.* on single forged W-UHP (ultra-high-purity-tungsten) of 5 mm thickness where cracks developed at relatively low heat fluxes ($>12\ \mathrm{MJ\,m^{-2}\,s^{-1/2}}$) and an equal number of pulses [10]. Crack networks were also observed after exposure of these samples (and double forged pure W) to 100 electron beam transients in the JUDITH 1 facility at FZJ which shows the loading methods to yield similar damage [6, 23].

Heat shock tests using the e-beam have been repeated on our samples (polycrystalline rolled W) and on W-UHP, both exhibiting a thickness of 1 mm in this case. Similar exposure conditions as in series B were applied: 100 transients, $F_{HF} =$ 20-40 $\mathrm{MJ\,m^{-2}\,s^{-1/2}}$ while the target base temperature was held at RT. Cracking was found absent in these tests [24]. Since it is demonstrated earlier that laser and e-beam loading yield similar surface damage [10], the absence of cracking for our samples appears likely to be a result of the metallurgical process (rolling) with which the samples were

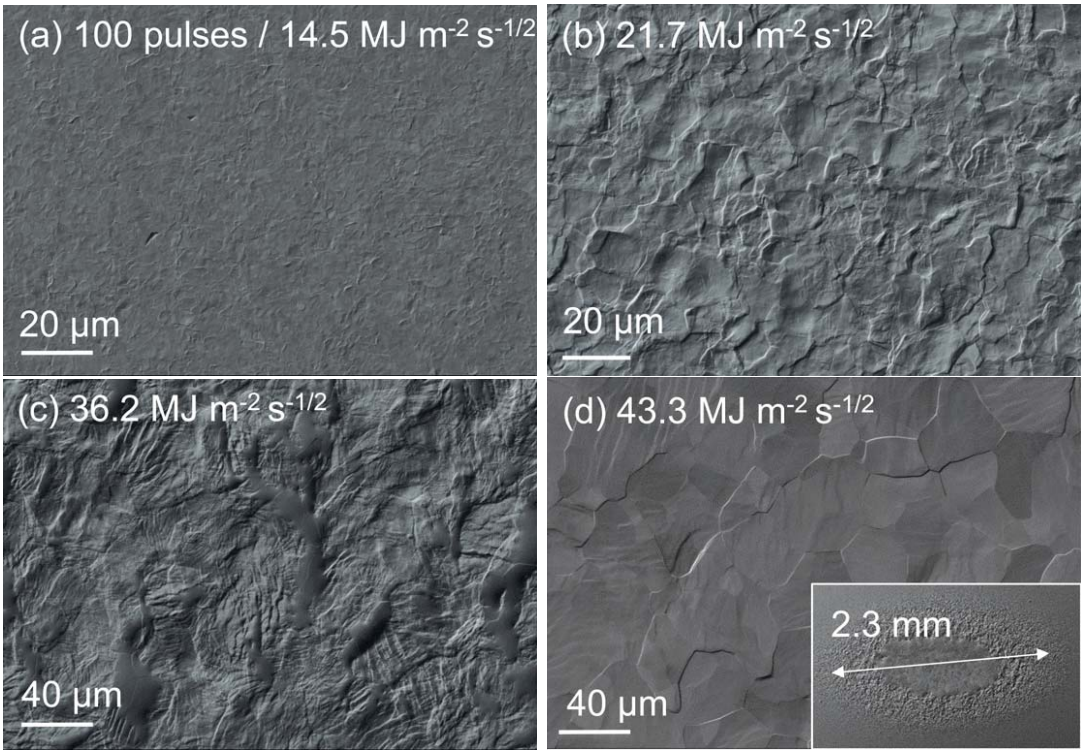

Figure 5: SEM images of surface morphology of W samples after being irradiated by 100 laser pulses at heat flux parameters as indicated.

manufactured and/or an effect of its thickness. The effect of the latter, as revealed in the case of W-UHP, needs further investigation as no detailed study of the influence of thickness is performed for the type of W under consideration in this report. It is however likely that the target thickness will affect the thermal stresses that may lead to crack formation.

In order to assess the influence of plasma exposure on the thermal shock damage of W, simultaneous exposures of laser and plasma have been performed. The total H fluence and base temperatures (T_{base}) are stated in table 1. As the base temperature of the samples is elevated during steady-state plasma, a lower heat flux parameter is expected to be sufficient to melt the surface compared the laser only exposures at RT. This difference due to the exposure method is taken into account by considering instead the peak temperatures (within the spatial limit down to 150 µm) to reach melting for both plasma and non-plasma exposures.

SEM images of the surface inside the laser spots are compared for the laser only and laser+plasma cases in figure 6 at peak temperatures ranging 2050-2450 °C. From this, it is found from 6d and 6b that melting is more extensive in the case of plasma presence compared to laser transients alone even if the peak temperatures reached are similar: the sample that was simultaneously exposed to plasma showed a contiguous melted patch of 100 µm in diameter whereas the areas that melted on the laser-loaded sample were limited to a few isolated grains of typically 20 µm.

Furthermore, individual grains are observed to melt at a measured peak temperature of ∼2260 °C when exposed to plasma and transients at $F_{HF} = 32.2$ MJ m^{-2} s$^{-1/2}$ (figure 6c). This temperature is significantly lower than in the laser only case where onset of melting was observed at ∼2480 °C and $F_{HF} = 36.2$ MJ m^{-2} s$^{-1/2}$ (figure 6b). Plasma presence is thus seen to reduce the heat flux parameter to reach the melting threshold in comparison to the situation without plasma.

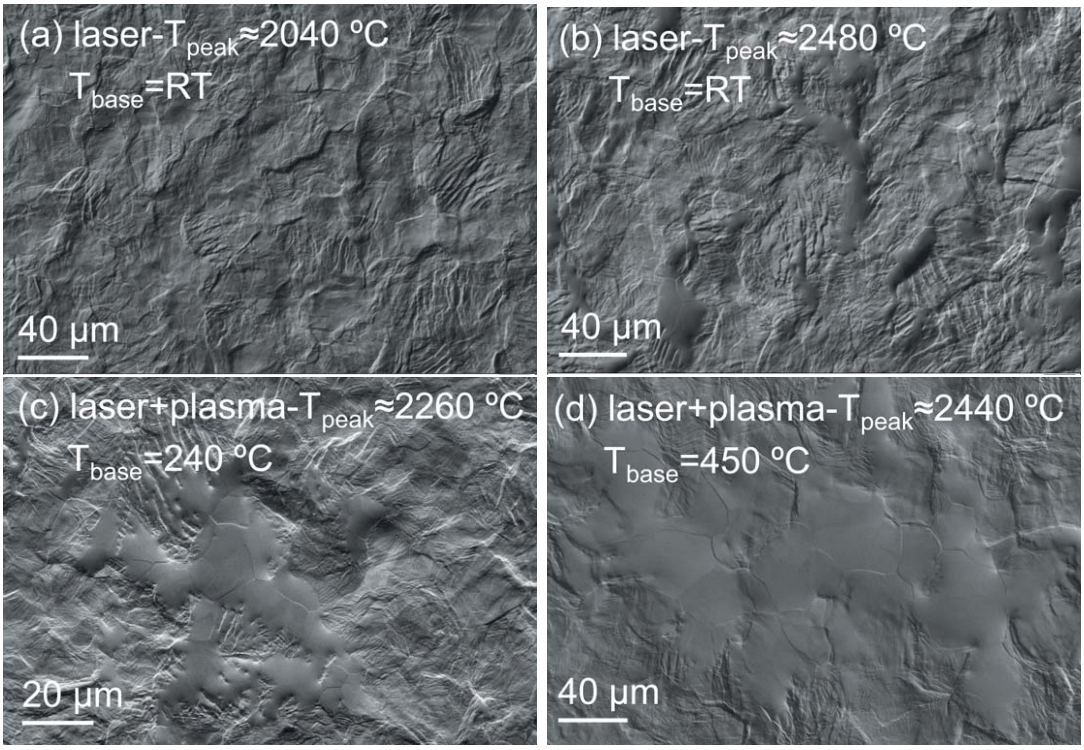

Figure 6: SEM images of W surface morphology after being irradiated by 100 pulses at 28.9 MJ m^{-2} s$^{-1/2}$ (a) and 36.2 MJ m^{-2} s$^{-1/2}$ (b) and exposed to plasma and laser simultaneously at 32.2 MJ m^{-2} s$^{-1/2}$ (c) and 25.2 MJ m^{-2} s$^{-1/2}$ (d).

3.2. Roughness and grain growth

The induced surface roughening as a result of laser pulses alone is shown in figure 7a (series A and B). It can be inferred from this that surface roughening due to impact of 100 transients increases linearly with increasing heat flux parameter (i.e. peak temperature) for heat flux parameters >15 MJ m^{-2} s$^{-1/2}$. The effect of the number of pulses was only investigated at $F_{HF} = 37.5$ MJ m^{-2} s$^{-1/2}$ which modified the surface already after only a single pulse to a similar roughness level as 100 pulses at $F_{HF} = 14.5$ MJ m^{-2} s$^{-1/2}$. The large R_a in cases of 1000 and 5000 pulses is due to crack formation. The influence of the loading method was assessed by cross-checking the profilometry data of our samples irradiated by the laser to similar samples exposed to e-beam pulses in the JUDITH-1 facility. Figure 7b shows similar roughness levels (and absence of cracking was found) which shows the agreement between these loading methods. The trend in roughening

as function of heat flux parameter is however not the same which is likely to be a result of the fast scanning procedure by the e-beam (as opposed to uniform irradiation by the laser) which leads to additional small thermal shocks and hence additional surface modifications.

The evolution of the surface roughness is plotted as a function of the transient peak temperature in figure 7b. By doing so, the laser only case can be compared to the exposures to plasma and laser simultaneously in terms of roughness evolution. Results of laser only (series A and B), loading on a heated sample at 450 °C (series C), and laser loading combined with plasma exposure (series E-H) as function of peak temperature and the number of pulses are shown. It is striking to see that nearly all data points lie on the same fitted line for temperatures >1100 °C. Hence, transient peak temperature is seen to drive surface roughening, regardless of plasma presence and base temperature.

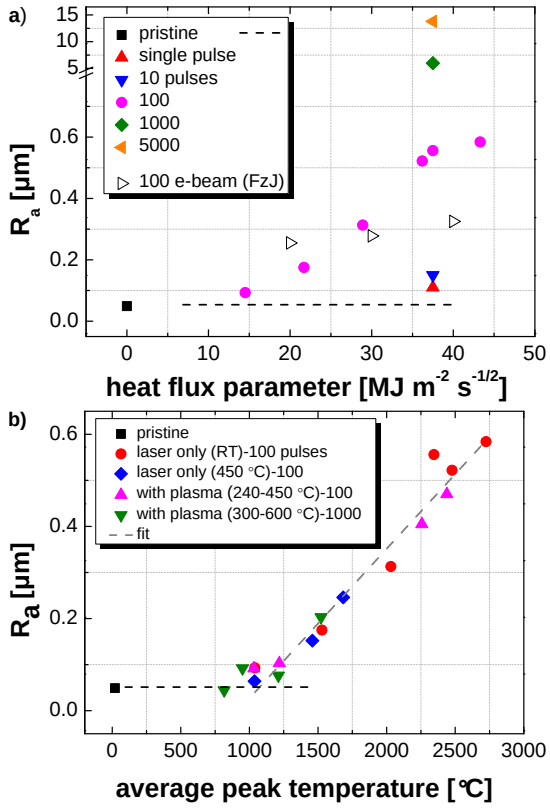

Figure 7: Mean roughness parameter (R_a) as function of heat flux parameter and number of pulses at the laser irradiated area without plasma at RT (a). R_a at the laser position as function of peak temperature of the laser pulses with and without plasma presence (b). The base temperature during exposure is indicated between brackets.

A strong dependency of roughness with the number of pulses is observed when loading at 37.5 $\mathrm{MJ\,m^{-2}\,s^{-1/2}}$ in the laser only case at RT as shown in 7a. Such dependency is however not found at 1200 °C in 7b where plasma/laser exposures to 100 and 1000 pulses yield similar roughness values. This result is likely to be attributed

to the low peak temperatures reached during the latter experiments, rather than an effect caused by the plasma.

Figure 8a shows the average surface grain size as function of heat flux parameter and the number of pulses for the laser only case. The grain size as function of transient peak temperature during plasma presence are shown in figure 8b and the data points of 100 laser pulses without plasma are plotted for comparison. Similarly to what is observed for the surface roughness evolution, grain growth at the surface is a function of both peak temperature and the number of pulses and starts for temperatures higher than 1500 °C, which is above the recrystallization temperature of W (1300-1500 °C), as expected. Grain growth is thus seen to be solely driven by the temperature reached during the transient, independent from the loading conditions.

A small discrepancy is observed in figure 8b at 1500 °C between the plasma and non-plasma cases. It is suggested that a slight difference in target cooling for these experiments affected the after-transient cooling rate, therefore changing the duration in which grain growth can occur. Apart from this, plasma exposure seems to have little effect on grain growth. Furthermore, grain growth is found to occur rapidly: within 1 ms (1 pulse) at 37.5 $\mathrm{MJ\,m^{-2}\,s^{-1/2}}$. By comparing the grain size in the centre after 1 pulse with that after 5000 pulses at this heat flux parameter, grains are found to grow by a factor ∼3.

3.3. Power handling

Measurable increases in ΔT during application of ELM-like pulses - assuming a constant heat flux parameter - are an indication of a reduction in thermal properties, as can be inferred from equation (2). Therefore, measuring the transient temperature evolution provides a tool to assess the power handling capabilities of the damaged W surface.

For irradiation at $\mathrm{F_{HF}}$ >15 $\mathrm{MJ\,m^{-2}\,s^{-1/2}}$ and $\mathrm{F_{HF}}$ >20 $\mathrm{MJ\,m^{-2}\,s^{-1/2}}$, for plasma+laser and laser only cases respectively, ΔT was found to increase with the number of pulses at fixed laser energy. At the end of the series of pulses, the measured temperature deviates from the predicted temperature by up to ∼100 °C in some cases. The increase in ΔT is illustrated in figure 9 where 50 laser pulses at $\mathrm{F_{HF}} =$ 25.2 $\mathrm{MJ\,m^{-2}\,s^{-1/2}}$ are applied in combination with steady-state plasma exposure. The slight decrease in base temperature through the discharge is due to a diminishing magnetic field strength leading to a decrease in power input to the plasma [13, 25]. This should have no effect on the transient temperature rise induced by the laser.

The actual heat flux parameter deposited on the surface during the last set of pulses can be corrected for the change in absorbance using equation (1). Peak temperatures are averaged over a set of 10 pulses for the 100 pulse cases, while an average over 50 pulses is done for the 1000 pulse cases. From this, one can correct the final temperature increase $\Delta\mathrm{T_f}$ (last set of pulses) for changes in laser absorbance and normalize it to the initial temperature increase $\Delta\mathrm{T_0}$ (first set of pulses).

Figure 10 shows $\Delta\mathrm{T_f}/\Delta\mathrm{T_0}$ versus the initial peak temperature ($\mathrm{T_{peak,0}}$ =

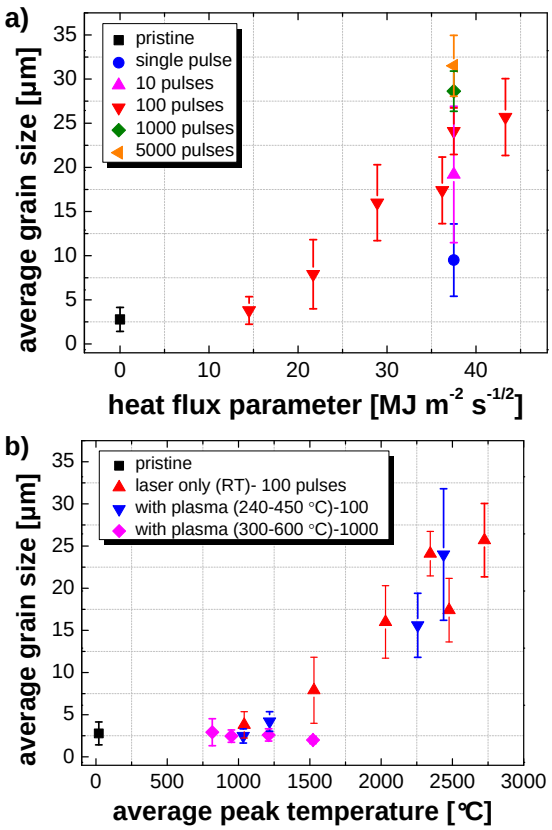

Figure 8: Average grain size in the centre of the laser deposited surface of the non-plasma exposed samples as function of applied heat flux parameter (series A and B) (a). Grain sizes in the centre of the laser spot after being exposed to transients and plasma at several base temperatures are compared to the laser only case for 100 pulses (series D-G) (b).

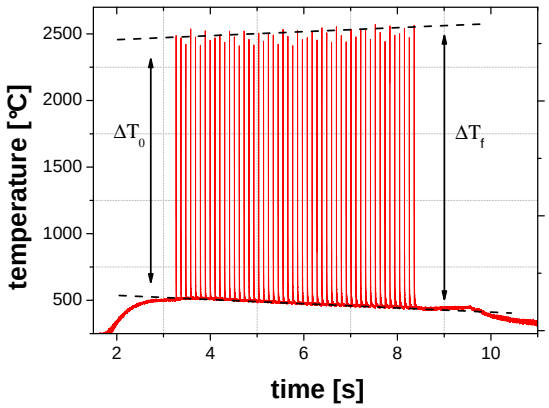

Figure 9: Temperature evolution at the centre of the laser deposited area during simultaneous plasma and laser exposure at 25.2 MJ m^{-2} s$^{-1/2}$ from fast IR analysis. ΔT is found to increase over the course of 50 pulses.

$T_{base}+\Delta T_0$) for targets both in absence and presence of plasma for 100 and 1000

pulses (series B-D and E-G). From this data, it can be inferred that ΔT increases by

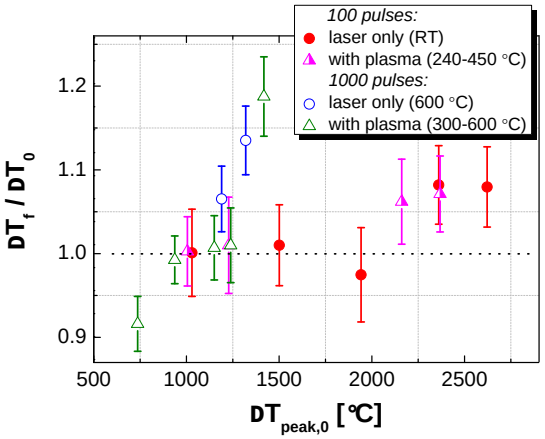

Figure 10: Change in ΔT for the final set of pulses (ΔT_f) relative to the first set of pulses (ΔT_0) as function of the initial peak temperature. A correction for changes in absorbance at the damaged surface is applied.

7-8 % over the course of 100 pulses when $T_{peak,0}$ >2000 °C. This corresponds to heat flux parameters >36 MJ m^{-2} s$^{-1/2}$ for the laser only case and >25 MJ m^{-2} s$^{-1/2}$ for plasma+laser irradiation.

With the succession of 1000 pulses, ΔT is found to increase at lower values of $T_{peak,0}$ compared to the 100 pulse exposures. The changes in reflectivity were not measured for these high pulse number exposures. However, at the peak temperatures that were reached during those experiments (1200-1800 °C), roughness levels similar to the 100 pulse exposures were obtained (figure 7b). The changes in reflectivity are therefore also assumed to be similar to the 100 pulse exposures at these peak temperatures: ∼10 % deviation from the pristine reflectivity value (corresponding to F_{HF} ∼25 MJ m^{-2} s$^{-1/2}$ in figure 3). Taking this into account, ΔT_f is seen to increase by 20 % relative to ΔT_0 at a moderate $T_{peak,0}$ of ∼1500 °C in plasma presence. In absence of plasma, ΔT was found to rise by 6 % relative to ΔT_0 for $T_{peak,0} \approx 1200$ °C and up to 14 % for $T_{peak,0} \approx 1320$ °C.

As changes in absorbance are taken into account for all data points in figure 10, the thermophysical properties of the damaged surface seem to deteriorate both as function of the number of pulses and as function of peak temperature. The increase in $\Delta T_f/\Delta T_0$ is highest for the 1000 pulse cases at low values of $T_{peak,0}$. ΔT was found unchanged during application of only 100 pulses in this temperature range and the roughness levels associated to these exposures are lower then those from the exposures >2000 °C as shown in figure 7b. A peak temperature >1100 °C is high enough for roughening to develop but apparently needs to exceed 100 pulses in order to accumulate lattice distortions and thermal fatigue to such an extend that it affects the surface heat dissipation capability [26].

Furthermore, as described earlier, the measured surface temperature from IR is the

average temperature over the size of a single pixel: ∼150 µm. Although measuring local melting of individual grains directly is impossible, the increase in melted area leads to an increased measured (average) temperature. The increase in melted surface fraction does not lead to an increased absorbance, as the resolidified surface was found to exhibit a higher reflectivity (figure 3). Hence, the rise of $\Delta T_f/\Delta T_0$ for the cases of $T_{peak,0}$ >2000 °C are likely to be partly attributed to the increase in melted area resulting from a reduced heat handling capability of the surface.

Figure 11 shows the evolution of ΔT with the number of pulses for the cases of 1000 pulses in which $\Delta T_f/\Delta T_0 > 1.05$. Although it is found that both the plasma and non-plasma cases show a similar evolution of ΔT with the number of pulses, the absolute increase in ΔT is highest for the plasma+laser case. This is likely due to higher $T_{peak,0}$ compared to the non-plasma cases: ∼1420 °C versus ∼1190/1320 °C. The peak temperature in these cases (1300-1500 °C) is in the regime of W where roughening occurs (figure 7). The significant rise in ΔT is therefore explained by a deterioration of thermal properties of the W surface due to repetitive plastic deformation rather than a plasma-induced effect taking place at the W surface. The thermal cycling leads to a loosening of grains which reduces the conductive heat transfer between the surface facing the plasma and the bulk. Hence, the reduction in power handling is a function of peak temperature and time, again independent of the loading method.

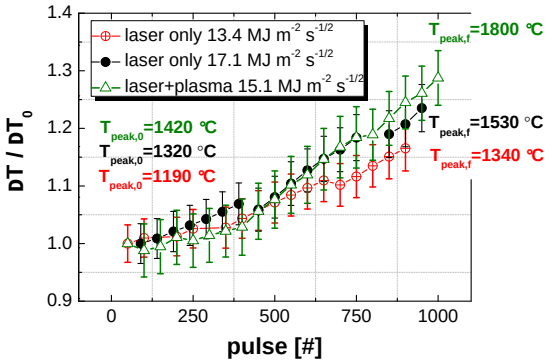

Figure 11: Evolution of ΔT normalized to ΔT_0 as function of the number of pulses for a total of 1000 transients. Exposure of externally heated samples at 600 °C in absence of plasma are compared to the plasma exposed case at similar base temperature. The initial and final peak temperatures are indicated.

3.4. Comparing exposure methods

Figure 12a shows the surface damage qualitatively as a result of pulsed laser irradiation for base temperatures ranging from RT to 600 °C. Damage of samples simultaneously exposed to H plasma at base temperatures 240-600 °C are shown figure 12b. In addition, results from samples pre-exposed to a deuterium (D) plasma up to a fluence of $\sim 4\times10^{26}\,m^{-2}$ and subsequently exposed to laser pulses were previously reported in [27]

and are shown in 12b for comparison (data points at RT). The parameter space that does not lead to significant damage for the laser only case is shown in this figure by the vertical fill pattern. The roughened and recrystallized surfaces of initially pristine W are indicated by the diagonal fill pattern.

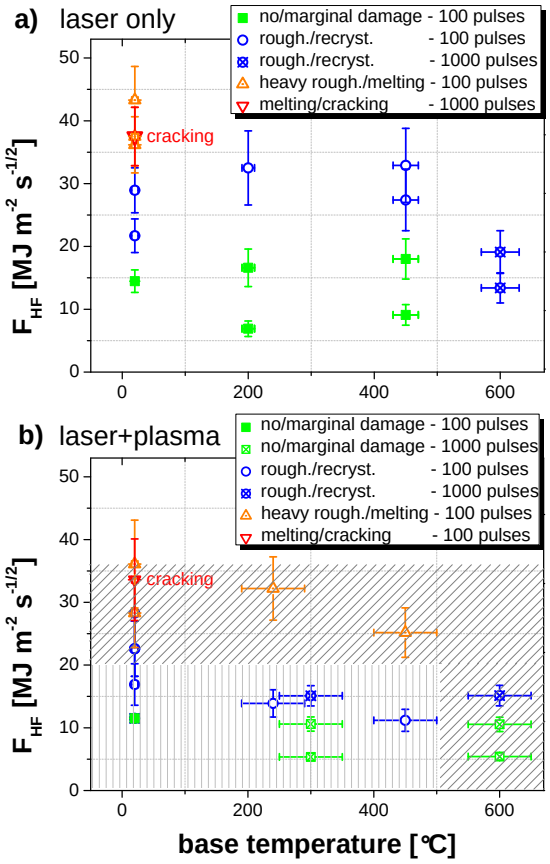

Figure 12: Qualitative surface damage of W after irradiation by 100-1000 laser pulses (a). Damage of targets pre-exposed to D plasma subjected to laser pulses (T_{base} =RT) and simultaneous H plasma/laser exposure (T_{base} >RT) (b). Data points in green indicate the absence of surface modifications up to very marginal roughening. Recrystallization and grain growth is shown in blue, pronounced recrystallization and the onset of melting in orange and red points indicate fully melted and cracked surfaces.

When comparing the damage effect at RT for the laser on a pristine W surface (12a) to that on a surface pre-exposed to D plasma (12b), the heat flux threshold to reach melting is found lowered for the latter case. For the pre-exposed surface, melting is observed for heat fluxes >28 MJ m^{-2} s$^{-1/2}$ whereas this is >36 MJ m^{-2} s$^{-1/2}$ for the pristine case.

Regarding cracking, a sample pre-exposed to a D fluence of 2.9×10^{26} m^{-2} cracked after applying 100 pulses at 33.6 MJ m^{-2} s$^{-1/2}$ whereas exposure of pristine samples to laser or e-beam pulses did not lead to cracking at all after this number of repetitions. Also, no cracking occurred after combined irradiation at a slightly higher

heat flux parameter of 36.1 MJ m^{-2} s$^{-1/2}$ with a lower D fluence of 2.1×10^{26} m^{-2}. A dependence of the cracking threshold on plasma fluence is expected from this, implying an embrittlement effect due to the pre-treatment of D plasma.

However, no cracking occurred on any of the samples exposed to laser+plasma and on the heated samples without plasma, even after 1000 pulses. Hence, no plasma induced embrittlement effect is found in the simultaneous plasma and laser cases. This observation is attributed to, firstly, the fact that these samples were above the Ductile to Brittle Transition Temperature (DBTT) during exposure, which prevented crack formation. Secondly, the maximum H fluence reached during the simultaneous exposures was an order of magnitude lower (1.5×10^{26} m^{-2}) than the maximum fluence reached in sequential exposures, which may be too low to increase embrittlement significantly.

For the simultaneous exposure to H plasma and laser pulses, extensive melting occurred for heat fluxes >25 MJ m^{-2} s$^{-1/2}$ at 450 °C base temperature, contrasting to the damage observed without plasma exposure where only roughening was to be seen. Also, the onset of melting was observed when exposing to $F_{HF} = 33.2$ MJ m^{-2} s$^{-1/2}$ at 240 °C base temperature with plasma presence while the sample unexposed to plasma revealed a non-melted roughened surface. In general, for $F_{HF} = 10$-20 MJ m^{-2} s$^{-1/2}$ and base temperatures of 200-500 °C, roughening (no melting) occurred on the surface of samples exposed to plasma+laser whereas the surface of samples exposed only to the laser were not significantly modified.

Because the applied heat flux parameters on the samples at 600 °C were below ∼20 MJ m^{-2} s$^{-1/2}$, the peak temperatures reached were too low to induce surface melting. Surface roughening was however found to develop to similar levels at these conditions for both the plasma and non-plasma cases. It must be noted that the number of pulses was high (1000) which leads to a thermo-mechanical fatigue effect which is not pronounced in the 100 pulse case, which explains the similarity in roughness. Despite this, the reduction of the melting threshold due to plasma presence is likely to be governed by a similar mechanism at 600 °C base temperature as was observed for base temperatures of 240 °C and 450 °C. It can thus be stated that the pre- and simultaneous exposure of W to a high density H plasma leads to a lowered heat flux parameter threshold to reach melting of W targets, at least for base temperatures ≤ 450 °C.

4. Conclusion and outlook

The main observations in this study are that, firstly, the presence of a high-flux H plasma induces melting at lower heat flux parameters in comparison to transients applied in absence of plasma. Next, transient-induced roughness, both in presence and absence of plasma, can be approximated by a single line that gives roughness as function of the transient peak temperature. The latter parameter is therefore found to act as an ordering parameter in terms of the roughness development and grain growth, rather than the exposure conditions and the target base temperature. Roughening and grain growth in response to repetitive ELM-like heating are found to occur above temperature

thresholds of 1100 °C and 1500 °C respectively independent of plasma presence.

Furthermore, an increase in temperature rise (ΔT) per successive pulse as function of heat flux parameter and number of repetitions is observed. By accounting for changes in absorbance of the laser light at the damaged surface, a reduction in power handling capability of the damaged W is concluded during exposure to 100 and 1000 transients at initial peak temperatures >2200 °C and >1200 °C respectively. Changes in power handling of the surface seems also driven by peak temperature and the number of pulses (exposure time) independent of plasma presence and base temperature. It is proposed that repetitive loading leads to a loosening of grain cohesion and thus a decrease in thermo-mechanical properties. This mechanism would also fit with the observations of below melting threshold melting and the increase of the melted region with the number of pulses.

Although similar in terms of pulse length and energy deposition to type-I ELMs, by using a pulsed laser some differences clearly exist between this experiment and real ELM loading. Discrepancies in spatial and temporal profile shapes, and no inclusion of the keV ion energy bombardment may affect somewhat differently the modification of the surface and its thermo-mechanical properties. Nonetheless, the observed evolving change in physical properties due to transient heating associated with ELMs should remain true. Transients leading to temperature rises on the PFCs above even 1200 °C appear likely to produce surface modifications and reduced heat dissipation properties. In turn, deterioration of PFC heat handling capability leads to increasing peak temperatures at constant ELM power flux, hereby further damaging the PFC surface in response to ELMs. Considering that the number of transients investigated here would be reached within only a few ITER discharges, a reduction of W power handling with progressing ELM number for conditions as reported here could be problematic for large-scale fusion devices as the effective lifetime of the W PFCs may be considerably reduced.

5. Acknowledgments

This work is part of the research program of the Stichting voor Fundamenteel Onderzoek der Materie (FOM), which is financially supported by the Nederlandse Organisatie voor Wetenschappelijk Onderzoek (NWO). It is supported by the European Communities under the contract of Association between EURATOM and FOM and was conducted within the framework of the European Fusion Programme. The work carried out at IPP was supported by Czech Science Foundation grant no. 14-12837S. The views and opinions expressed herein do not necessarily reflect those of the ITER Organization.

References

[1] Loarte A, Huijsmans G, Futatani S *et al.* 2014 *Nucl. Fus.* **54** 033007
[2] Loarte A, Saibene G, Sartori R *et al.* 2007 *Phys. Scr.* **T128** 222
[3] Leonard A W 1999 *J. Nucl. Mat.* **266-269** 109–117

[4] Pintsuk G 2012 *Tungsten as a Plasma-Facing Material* (*Comprehensive Nuclear Materials* no 438) (Spain: Elsevier)
[5] Pitts R A, Carpentier S, Escourbiac F *et al.* 2013 *J. Nucl. Mat.* **438** S48–S56
[6] Linke J, Loewenhoff T, Massaut V *et al.* 2011 *Nucl. Fus.* **51** 073017
[7] Loewenhoff T, Bürger A, Linke J *et al.* 2011 *Phys. Scr.* **T145** 014057
[8] Wirtz M, Linke J, Pintsuk G *et al.* 2013 *J. Nucl. Mat.* **443** 497–501
[9] Umstadter K R, Doerner R and Tynan G 2009 *J. Nucl. Mat.* **386-388** 751–755
[10] Wirtz M, Linke J, Pintsuk G *et al.* 2013 *J. Nucl. Mat.* **438** S833–S836
[11] Loewenhoff T 2012 *Combined Steady-state and High Cycle Transient Heat Load Simulation with the Electron Beam Facility JUDITH 2 (PhD thesis)* (Rheinisch Westfälischen Technischen Hochschule Aachen)
[12] Zielinski J J, van der Meiden H J, Morgan T W *et al.* 2014 *Appl. Phys. Lett.* **104** 124102
[13] Temmerman G D, van den Berg M A, Scholten J *et al.* 2013 *Fus. Eng. Des.* **88** 483–487
[14] van Eck H J N, Kleyn A W, Lof A *et al.* 2012 *Applied Physics Letters* **101** 224107
[15] van der Meiden H J, Lof A R, van den Berg M A *et al.* 2012 *Rev. Sci. Instrum.* **83** 123505
[16] Roberts S 1959 *Phys. Rev.* **114** 104–115
[17] Gadelmawla E S, Koura M M, Maksoud T M A *et al.* 2002 *Journal of Materials Processing Technology* **123** 133–145
[18] Linke J, Escourbiac F, Mazul I V *et al.* 2007 *J. Nucl. Mat.* **367-370** 1422–1431
[19] Hirai T, Pintsuk G, Linke J *et al.* 2009 *J. Nucl. Mat.* **390-391** 751–754
[20] Lassner E and Schubert W D 1999 *Tungsten Properties, Chemistry, Technology of the Element, Alloys and Chemical Compounds* 1st ed (US: Springer)
[21] Kajita S, Temmerman G D, Morgan T W *et al.* 2014 *Nucl. Fus.* **54** 033005
[22] Huber A, Arakcheev A, Sergienko G *et al.* 2014 *Phys. Scr.* **T159** 014005
[23] Wirtz M, Linke J, Pintsuk G *et al.* 2011 *Phys. Scr.* **T145** 0140058
[24] Wirtz M 2014 *private communication*
[25] Scholten J, Zeijlmans van Emmichoven P A, van Eck H J N *et al.* 2013 *Fus. Eng. Des.* **88** 1785 – 1788
[26] Loewenhoff T, Linke J, Pintsuk G *et al.* 2012 *Fus. Eng. Des.* **87** 1201–1205
[27] Morgan T W, Zielinski J J, Hensen B J *et al.* 2013 *J. Nucl. Mat.* **438** 784–787